Reference: *Biol. Bull.* **229:** 185–198. (October 2015)

Flexibility of Crab Chemosensory Sensilla Enables Flicking Antennules to Sniff

LINDSAY D. WALDROP[1,*,†], MATTHEW A. REIDENBACH[2], AND M. A. R. KOEHL[1]

[1]*Department of Integrative Biology, University of California, Berkeley, California 94720-3140; and*
[2]*Department of Environmental Sciences, University of Virginia, Charlottesville, Virginia 22904*

Abstract. The first step in smelling is capture of odorant molecules from the surrounding fluid. We used lateral flagella of olfactory antennules of crabs *Callinectes sapidus* to study the physical process of odor capture by antennae bearing dense tufts of hair-like chemosensory sensilla (aesthetascs). Fluid flow around and through aesthetasc arrays on dynamically scaled models of lateral flagella of *C. sapidus* was measured by particle image velocimetry to determine how antennules sample the surrounding water when they flick. Models enabled separate evaluation of the effects of flicking speed, aesthetasc spacing, and antennule orientation. We found that crab antennules, like those of other malacostracan crustaceans, take a discrete water sample during each flick by having a rapid downstroke, during which water flows into the aesthetasc array, and a slow recovery stroke, when water is trapped in the array and odorants have time to diffuse to aesthetascs. However, unlike antennules of crustaceans with sparse aesthetasc arrays, crabs enhance sniffing *via* additional mechanisms: 1) Aesthetascs are flexible and splay as a result of the hydrodynamic drag during downstrokes, then clump together during return strokes; and 2) antennules flick with aesthetascs on the upstream side of the stalk during downstrokes, but are hidden downstream during return strokes. Aiming aesthetascs into ambient flow maintains sniffing. When gaps between aesthetascs are wide, changes in antennule speed are more effective at altering flow through the array than when gaps are narrow. Nonetheless, if crabs had fixed gap widths, their ability to take discrete samples of their odorant environment would be diminished.

Received 30 December 2014; accepted 15 May 2015.

* To whom correspondence should be addressed. E-mail: lwaldrop@ucmerced.edu

† Present address: School of Natural Sciences, University of California, Merced, Merced, California 95343.

Introduction

Many animals from different phyla use olfactory appendages bearing arrays of hair-like structures to perform important functions, such as locating food or suitable habitats, identifying mates or competitors, and sensing predators (Atema, 1995; Moore and Crimaldi, 2004; Webster and Weissburg, 2009). The first step in the process of smelling is interception of odor molecules carried in the surrounding fluid by these olfactory organs. To understand the mechanisms by which organisms capture odors from the environment, we must study how olfactory organs interact with the water or air around them. The olfactory antennules of aquatic crustaceans are useful systems for studying the physical process of odor capture, because antennules protrude into the water where we can measure their interactions with the fluid environment.

Olfactory antennules

Antennules are olfactory organs involved in detection of odorants that stimulate upstream locomotion and tracking of distant odor sources by diverse malacostracan crustaceans (*e.g.,* Devine and Atema, 1982; Atema, 1998; Mead, 2002; Mead *et al.*, 2003; Weissburg *et al.,* 2012; Moore and Kraus-Epley, 2013). One branch of an antennule, the lateral flagellum, bears rows of aesthetascs that contain the dendrites of chemosensory neurons that project to the olfactory lobes of the brain (reviewed by Ache, 1982, and Koehl, 2006; Ache and Derby, 1985; Grünert and Ache, 1988). The arrangement of aesthetascs on the lateral flagella of many brachyuran and marine anomuran crabs is a dense, flexible brush; these crabs flick the lateral flagella bearing this array through the water (*e.g.*, Snow, 1973; Koehl, 2006, 2011; Waldrop, 2013; Waldrop *et al.,* 2015).

It has long been suggested that when malacostracan crustaceans flick the lateral flagella of their antennules, they increase the penetration of ambient water into the spaces between the aesthetascs, thus bringing odor-carrying water closer to the surfaces of those aesthetascs (*e.g.,* Snow, 1973; Schmitt and Ache, 1979; Atema, 1985; Moore *et al.,* 1991; Gleeson *et al.*, 1993; Koehl, 1995, 1996; Pravin and Reidenbach, 2013; Waldrop *et al.*, 2014). Understanding how water samples are moved into the spaces between the hair-like aesthetascs is an important part of deciphering the process of capturing chemical signals from the environment.

Fluid flow through arrays of hairs

Fluid flow around a hair in an array depends on the relative importance of inertial and viscous forces, given by the Reynolds number (*Re*)

$$Re = \frac{UL\rho}{\mu} \qquad \text{(Equation 1)}$$

where U is the velocity of the fluid in relation to the hair, L is the hair diameter, ρ is the fluid density, and μ is the dynamic viscosity of the fluid (resistance of the fluid to being sheared) (*e.g.*, Vogel, 1994). Very small (low L) structures, such as an aesthetasc on an antennule, operate at low *Re's* and experience fluid motion that is laminar because viscous forces damp out disturbances to the flow.

Fluid in contact with the surface of a moving solid object does not slip in relation to the object's surface; hence, a velocity gradient develops in the fluid next to the object (*e.g.*, Vogel, 1994). The lower the *Re*, the thicker this boundary layer of sheared fluid in relation to the size of the body. If the boundary layers around hairs in a finite array are thick in comparison to the gaps between neighboring hairs, then fluid tends to move around rather than through the array. Calculation of the velocities of fluid flow around and between cylinders in arrays (Koehl, 1995, 2003; Pravin *et al*., 2012; Schuech *et al*., 2012) revealed that hair arrays undergo a transition from non-leaky behavior (where little fluid flows between adjacent hairs) to leaky, sieve-like behavior (where fluid flows between neighboring hairs) as *Re* increases. Mathematical models (Cheer and Koehl, 1987a, b) showed that for closely spaced hairs (like aesthetascs on many crustacean antennules), the transition in leakiness occurs in a critical range of *Re*'s, between 0.1 and 1, and that leakiness is very sensitive to the ratio of the width of the gap between neighboring hairs to hair diameter. Thus, the basic physical rules governing how arrays of hairs interact with fluids suggest that the velocity of antennule flicking, along with the size and spacing of aesthetascs, determine whether odor-bearing water flows through or around an array of aesthetascs.

Flicking is sniffing

Malacostracan crustaceans flick the lateral flagella of their antennules through the water in the *Re* range at which the leakiness of an array of hairs is very sensitive to velocity. During the rapid downstroke of the antennule flick of a variety of malacostracans, the aesthetascs operate at *Re*'s of approximately 1; and during the slower return stroke, the aesthetascs operate at *Re*'s of about 0.1 (stomatopod *Gonodactylus mutatus*: Mead *et al*., 1999; spiny lobsters of various species: Goldman and Koehl, 2001; Goldman and Patek, 2002; brachyuran crab *Hemigrapsis oregonensis*: Waldrop, 2013). Water flows between the aesthetascs during the downstroke, but flows around, not through, the array during the slower return stroke (*G. mutatus*: Mead and Koehl, 2000; *Panulirus argus*: Koehl, 2001a; Reidenbach *et al*., 2008; *H. oregonensis*: Waldrop *et al.,* 2015), lasting long enough for the odor molecules in the trapped water to diffuse to the surfaces of the aesthetascs (*G. mutatus*: Stacey *et al*., 2002; crayfish *Procambarus clarkii*: Pravin *et al*., 2012; *Panulirus argus*: Schuech *et al*., 2012). Each flick can be considered a "sniff," which takes a discrete sample of the fluid environment in space and time (*e.g.*, Schmitt and Ache, 1979; Schoenfeld, 2006; Koehl, 2011; Nelson *et al*., 2013; Waldrop *et al.*, 2015).

The short lateral flagella of the antennules of the anomuran marine hermit crab (Snow, 1973), the brachyuran blue crab (Gleeson, 1982), and the brachyuran shore crab (Waldrop, 2013) bear a densely packed array of aesthetascs that resemble a toothbrush (Fig. 1A–D). The aesthetascs of these crabs are flexible and are deflected during a flick (Snow, 1973; Waldrop, 2013). During the rapid downstroke (Fig. 1B), the aesthetascs that are on the upstream side of the lateral flagellum splay and the gaps between neighboring aesthetascs widen. In contrast, during the slow recovery stroke (Fig. 1C), when the aesthetascs are on the downstream side of the lateral flagellum, they are pushed closer together. For this study, we used the antennules of the blue crab *Callinectes sapidus* to study water flow around and through the brush-like tufts of densely packed aesthetascs. We examined how that flow is affected by aesthetasc flexibility, which changes inter-hair spacing between the downstroke and return stroke of a flick.

Antennules of the blue crab

The blue crab *Callinectes sapidus* Rathbun, 1896, lives in estuarine habitats where it is exposed to water of varying salinity (*e.g.*, Gleeson *et al.,* 1997). The cuticle of aesthetascs is permeable to both water and ions (Gleeson *et al*., 2000a, b), and to dissolved chemical cues. The blue crab uses these dissolved chemical cues for food, predator, and mate detection throughout its life. It also uses smells to track food sources in ambient water currents (Weissburg and Zimmer-Faust, 1994; Webster *et al.,* 2001; Keller *et al.,*

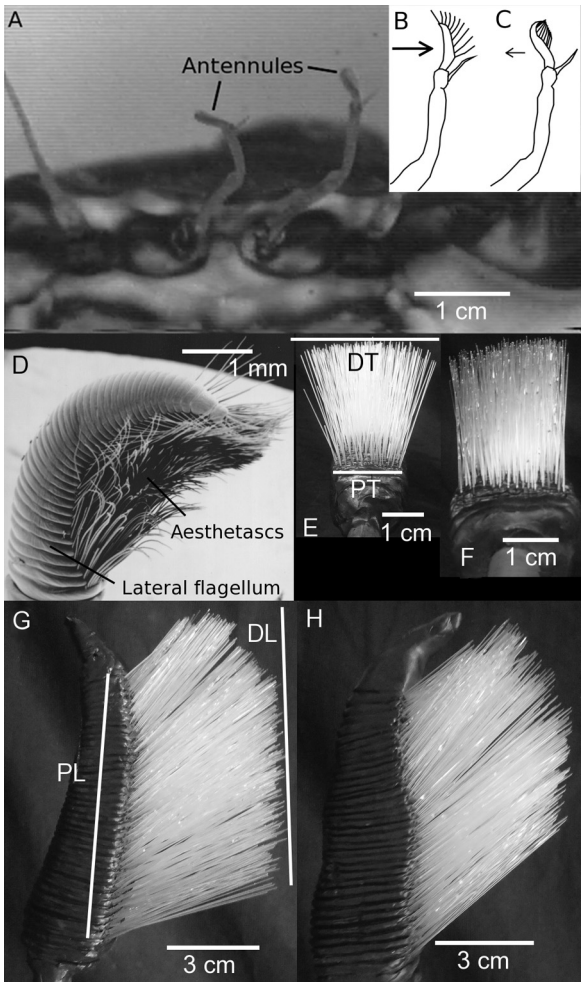

Figure 1. Olfactory antennules of the blue crab *Callinectes sapidus*. (A) Face-on view of an adult crab showing positions of the antennules. (B) Line drawing of the lateral flagellum of an antennule during the rapid downstroke of a flick, when the flagellum is flexed dorsally and the aesthetascs are splayed. The arrow shows the direction of antennule movement. (C) Line drawing of the lateral flagellum of an antennule during the slow return stroke of a flick, when the flagellum is flexed ventrally and the aesthetascs are clumped. The arrow shows the direction of antennule movement. (D) Scanning electron micrograph of the distal end of a lateral flagellum of an antennule and the aesthetasc array in the clumped configuration (as shown in (B)). (E) End-on view of a physical model of the lateral flagellum (black stalk) and aesthetasc array (light rods) in the splayed configuration of the antennule during the downstroke. The white line *DT* (distal transverse) shows the width of the aesthetasc array in the transverse direction at the distal tips of the aesthetascs; the white line *PT* (proximal transverse) shows the width of the array at the proximal end of the aesthetascs. The transverse splay ratio = *DT*/*PT*. (F) End-on view of a physical model of the lateral flagellum in the clumped configuration of the antennule during the return stroke. (G) Lateral view of a physical model of the lateral flagellum with the aesthetasc array in the splayed configuration. The white line *DL* (distal longitudinal) shows the length of the aesthetasc array at the distal tips of the aesthetascs; the white line *PL* (proximal longitudinal) shows the length of the array at the proximal end of the aesthetascs. The longitudinal splay ratio = *DL*/*PL*. (H) Lateral view of a physical model of the lateral flagellum in the clumped configuration.

2003; Dickman *et al.,* 2009; Page *et al.,* 2011a, b) and to mediate reproductive behaviors (Gleeson, 1980, 1982).

The morphology (Fig. 1D), physiology, and kinematics of the antennules of adult *C. sapidus* have been studied. The lateral flagellum of the antennule of a blue crab (Fig. 1D) is only about 2 mm long and bears a dense tuft of approximately 650–700 aesthetascs on its ventral surface (Gleeson, 1982). The aesthetascs are 700–1000 mm long 10–12 mm in diameter (Gleeson, 1982). Dendritic segments of chemosensory neurons extend within each aesthetasc and are bathed in sensillar lymph. This lymph is separated from the ambient water by the thin cuticle, which is permeable to odorants and to ions (Gleeson *et al.*, 2000a, b). Analysis of high-speed videos of flicking antennules of *C. sapidus* shows that crabs flick the lateral flagellum at a rate of 3 Hz. During the flick downstroke, the aesthetasc tuft sweeps through the water at a mean velocity of 0.17 m s^{-1}, traveling only a short linear distance (~4 mm); during the return stroke, the lateral flagellum moves more slowly, at a mean velocity of 0.06 m s^{-1}, and the antennule is stationary during a brief pause, lasting 0.24 s on average, before the next downstroke (Koehl, 2011; Reidenbach and Koehl, 2011; Waldrop, 2012). When *C. sapidus* is exposed to ambient water currents in a flume, it orients each antennule with its aesthetasc-bearing ventral surface pointing upstream and decreases the speed of the downstroke (Table 1). This behavior differs from that of crayfish, which increase antennular flick speeds in ambient currents (Moore and Kraus-Epley, 2013).

Objectives of this study

We used dynamically scaled physical models of the aesthetasc arrays on the lateral flagella of antennules of the blue crab *C. sapidus* to determine how these brush-like structures sample the water around them. The specific questions we addressed were as follows:

1) Do the antennules of blue crabs sniff (*i.e.*, take a discrete sample of water into the aesthetasc array during each flick)?
2) How is water flow through the array of aesthetascs affected by aesthetasc flexibility?
3) How does the location on the upstream *versus* the downstream side of an antennule affect the water flow through the aesthetasc array?
4) How does the difference in speed of the lateral flagellum during the rapid downstroke *versus* the slower upstroke affect water movement through the aesthetasc array?
5) When a crab in an ambient water current flicks its antennules, what is the water flow through an aesthetasc array during the downstroke and return stroke?

Table 1

Mean water speeds (±95% confidence intervals, n = 3 replicate runs) through the dendrite-bearing region of an aesthetasc array on the lateral flagellum of a Callinectes sapidus. *Oil speeds in the aesthetasc arrays of models of antennules were converted to water speeds in the aesthetasc arrays of real antennules operating at the same Reynolds number* (Re)

Antennule stroke	Downstroke			Return stroke		
Speed of antennule motion (cm s^{-1})[1]	17	16	15	6.1	6.5	5.0
Speed of ambient current (cm s^{-1})	0	4	15	0	4	15
Relative speed of antennule (cm s^{-1})[2]	17	20	30	6.1	2.5	10
Aesthetasc Re[3]	1.6	1.8	2.8	0.57	0.23	0.94
Mean water speed (cm s^{-1}) in splayed aesthetasc array[4]						
Array on upstream side of flagellum	1.43 ± 0.02	1.80 ± 0.1	3.62 ± 0.3	0.256 ± 0.2	0.256 ± 0.2	0.535 ± 0.02
Array on downstream side of flagellum	0.456 ± 0.06	0.623 ± 0.01	1.31 ± 0.2	0.0976 ± 0.03	0.0437 ± 0.01	0.174 ± 0.03
Mean water speed (cm s^{-1}) in clumped aesthetasc array[4]						
Array on upstream side of flagellum	0.949 ± 0.2	1.32 ± 0.3	2.51 ± 0.5	0.256 ± 0.2	0.0486 ± 0.02	0.413 ± 0.1
Array on downstream side of flagellum	0.129 ± 0.03	0.262 ± 0.2	0.535 ± 0.1	0.0398 ± 0.8	0.0269 ± 0.004	0.0619 ± 0.005

[1] *Re* (Equation 1) calculated using the net water velocity in relation to an antennule for *U* (vector sum of water velocity relative to antennule due to the flicking motion of the antennule and to an ambient water current), the aesthetasc diameter (8.5 mm) for *L*, and the density and dynamic viscosity of seawater at 20 °C ($\rho = 1.024 \times 10^3$ kg m^3, $\mu = 1.072 \times 10^{-3}$ kg m^{-1} s^{-1}; Vogel 1994).

[2] The kinematics of antennule flicking by *C. sapidus* in still water (Reidenbach and Koehl, 2011) and in flowing water in a flume (Martinez and Koehl, unpubl. data) was measured using the techniques described by Mead *et al.* (1999, 2003). The aesthetasc-bearing side of the lateral flagellum faced upstream in the ambient current. Thus, during the flick downstroke, the ambient current velocity was in the same direction as the water flow in relation to the antennule due to the downstroke motion. Hence, the net speed of water relative to the antennule during the downstroke was the sum of the magnitudes of those vectors. During the return stroke, the water flow due to antennule motion was in the opposite direction from the velocity of the ambient current past the antennule. Thus, the magnitude of the return stroke velocity was subtracted from the magnitude of the ambient current velocity to determine the net water speed relative to the antennule during the return stroke.

[3] Antennule speeds were measured on video records of antennule flicking by *C. sapidus* in still water or in a flume exposed to an ambient water current (M. Martinez, U. Lee, and M. Koehl, unpubl. data). The speed of the lateral flagellum of the antennule during both the downstroke (columns 2–4) and return stroke (columns 5–7) depended on the ambient water current velocity.

[4] For each run, we calculated the mean of the water speeds at the 6100 grid points within the dendrite-containing area of the aesthetasc array (shown by a white box in Fig. 3B, C, E, F). For each treatment, we calculated the grand mean of those mean water speeds ($n = 3$ replicate runs).

Materials and Methods

The fine-scale water flow in relation to arrays of microscopic aesthetascs on rapidly flicking crab antennules is very difficult to measure. Thus, we measured water velocities around and through the aesthetascs of large, dynamically scaled physical models of the lateral flagellum of the antennule of adult *Callinectes sapidus* (Fig. 1E–H). If a model is geometrically similar to a real antennule and operates at the same *Re*, then the model is dynamically similar to the antennule, and the ratios of velocities at comparable positions in the fluid around the model and the real antennule are the same (*e.g.*, Vogel, 1994; Koehl, 2003; Munk, 2011; Evangelista *et al*., 2014; Waldrop *et al.*, 2015).

Antennule models

Two geometrically scaled physical models were constructed of the lateral flagellum of a *C. sapidus* antennule, one with the aesthetascs splayed as they are during the downstroke of a flick (Fig. 1E, G), and one with the aesthetascs clumped together as on the return stroke (Fig. 1F, H). The dimensions of the lateral flagellum and aesthetascs, the orientation and number of aesthetascs in each row, and the number and spacing of rows of aesthetascs on each model flagellum were based on measurements made on scanning electron micrographs of adult *C. sapidus* (Koehl, 2011; Reidenbach and Koehl, 2011). The linear dimensions of the models were 70 times greater than those of the real antennules. The transverse and longitudinal "splay ratios" (SR; illustrated in Fig. 1E, G, respectively) of the splayed (SR = 2.19) and clumped (SR = 1.66) models were based on measurements of aesthetasc arrays in videos of flicking antennules of *C. sapidus.*

The lateral flagellum of each model (14 cm long) was constructed from Sculpey modeling compound (Polyform Products Co., Elk Grove Village, IL), and the aesthetascs were shaped from borosilicate glass rods (Pyrex; Corning, Inc., Lowell, MA) heated over a Bunsen burner and pulled to the correct diameter (0.7 mm). The glass aesthetascs were cut to the appropriate lengths and inserted into the Sculpey flagellum, and the model was then cured in a kiln at 80 °C for 40 min.

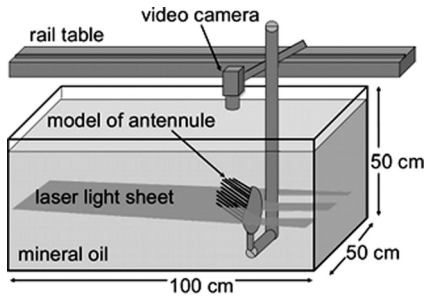

Figure 2. Diagram of the towing tank used for particle image velocimetry. A model of the lateral flagellum of a crab antennule was immersed in mineral oil containing neutrally buoyant reflective particles (11 mm in diameter), and towed along a rail parallel to the long axis of the tank by a programmable stepper-motor. A sheet of laser light illuminated a single plane of the fluid. In the configuration shown here, lasers were mounted on the side of the tank to produce a horizontal sheet of light that intersected a cross-section of a model flagellum at the midpoint along its length. A video camera was mounted on the rail system and was towed along with a model to record particles moving in relation to the model.

Towing apparatus

We operated our large models at the same *Re*'s as flicking antennules by moving them more slowly through a fluid that was more viscous than water. Models were towed through mineral oil with a density of 840 kg m^{-3} and a viscosity of 0.049 ± 0.002 Pa s (SD, $n = 3$), measured with a viscometer (Brookfield Inc., Middleboro, MA) at 25 °C, the temperature at which all experiments were conducted. The tank in which the models were towed (Fig. 2) was 100 cm long, 50 cm wide, 50 cm high; it contained 250 l of oil. The model was towed along a rail parallel to the long axis of the tank by a programmable stepper-motor (single-axis microstepping positioning system MC6023; Daedal, Inc., Irwin, PA); towing speed was controlled by voltage signals sent from a computer (for details, see Loudon *et al.*, 1994). Models were towed at velocities that matched the *Re*'s of a real antennule during the flick downstroke and return stroke in still fluid, or that matched the *Re's* of a real antennule with its aesthetasc-bearing ventral surface facing upstream in an ambient current of 0.04 m s^{-1} or 0.15 m s^{-1} during the downstroke or the recovery stroke (Table 1). The Pyrex glass aesthetascs had nearly the same refractive index (1.47) as that of mineral oil (1.46), allowing distortion-free visualization of the fluid flow through the optically transparent aesthetasc array.

Walls can affect the flow around an object at low *Re*, even when the object is many diameters away from the walls (*e.g.*, Loudon *et al.*, 1994). A rule of thumb for estimating when the effects of a wall on the flow around a body (such as an antennule) can be ignored is given by

$$\frac{y_w}{L_f} > \frac{20\nu}{L_f U_b} \qquad \text{(Equation 2)}$$

where y_w is the distance between the body surface and the wall, L_f is the diameter of the lateral flagellum at its widest point, U_b is the velocity of the body relative to the stationary fluid and wall, and ν is the kinematic viscosity of the fluid (Vogel, 1994). For our towing experiments, $L_f = 0.05$ m, $U = 0.02$ m s^{-1} for the lowest towing speed of the model (when wall effects would have been the greatest for our models), and $\nu = 5.8 \times 10^{-5}$ m^2 s^{-1}. Therefore, if $y_w >$ 0.06 m, wall effects were negligible in our experiments. Our models were towed at distances of $y_w \geq 0.12$ m from the walls of the tank.

The aesthetasc-bearing region along the lateral flagellum of *C. sapidus* is 2 mm long. Analysis of high-speed videos of *C. sapidus* antennules shows that during the flick downstroke, the aesthetasc array sweeps through an arc, moving a linear distance of approximately 4 mm. Since a flicking flagellum has a primary axis of rotation at the joint between the second and third segments of the peduncle of the antennule, the velocity of the flick varies linearly along the length of the antennule between that joint and the distal end of the aesthetasc array. Our model was towed at a velocity that produced the same *Re* as that of the midpoint of the aesthetasc array along the antennule, and we measured water flow in a plane that was normal to the model's long axis at the midpoint of the aesthetasc array. The average length between the joint at the second and third segments of the peduncle and the tip of the antennule is 1.4 cm. Therefore, the most proximal end of the aesthetasc array on a real antennule moves more slowly than the midpoint, and the distal tip moves more rapidly than the midpoint, each by a factor of only about 0.075, since the aesthetasc array is so short. These velocity differences along the length of the aesthetasc array were smaller than the SD values of the velocities measured during our experiments, so the flow measured at the midpoint is a good approximation of the flow for the whole aesthetasc array.

Although antennules accelerate at the start and decelerate at the end of each stroke during the flick, our experiments were performed at single downstroke or return stroke velocities, thereby assuming steady-state conditions. The relative importance of unsteady inertial (accelerational or decelerational) forces to viscous forces can be quantified through the dimensionless Womersley number (*Wo*), defined as

$$Wo = 0.5L\sqrt{\frac{2\pi f}{\nu}} \qquad \text{(Equation 3)}$$

where L is the characteristic spacing between aesthetascs, and v is the kinematic viscosity (Loudon and Tordesillas, 1998). For $W_O < 1$, unsteady inertial forces become negligible and viscosity dominates. For flows between the splayed aesthetascs during a downstroke ($L = 8.9 \pm 4$ μm), $W_O = 0.02 \pm 0.01$ and is even lower during the return

stroke. Such low W_O's indicate that the flow within the aesthetasc-bearing region of the antennule is not appreciably affected by accelerations or decelerations, and thus may reasonably be approximated by a flow relative to a model towed at a constant velocity. In addition, kinematic analysis of the flicking crab antennule shows that during the downstroke or return stroke, the antennule travels at a constant speed at least 90% of the time (Martinez and Koehl, unpubl. data).

Particle-image velocimetry

Video records of fluid motion surrounding the antennule model and through the aesthetasc array were made using a Particle Image Velocimetry (PIV) system. A sheet of laser light was used to illuminate a single plane of the fluid. The 2-mm thick light sheet was produced by a row of six red (670 nm) laser diodes with cylindrical beam expanders (World Star Tech, North York, ON, Canada). Since the model flagellum's length was 14 cm, the thickness of the laser light sheet was less than 1.5% of the length of the aesthetasc region of the model. These lasers were mounted on a rigid plate attached to a calibrated microscope stand that was used to adjust plate position to the nearest 0.2 mm. The lasers were mounted on the side of the tank to produce a horizontal sheet of light that intersected a cross-section of a model flagellum at the midpoint along its length (Fig. 2). The lasers were also mounted at the end of the tank to produce a vertical sheet of light parallel to the long axis of the model along the midline of the model flagellum.

The mineral oil was seeded with neutrally buoyant, reflective, silver-coated, hollow glass spheres (Potter Industries, Malvern, PA), which were 11 mm in diameter. The density of these particles varied slightly; some rose or sank at velocities no greater than 0.2 mm s^{-1}. Since horizontal velocities of the particles using pairs of video frames were taken over a period of only 0.03 s, the sinking or rising of particles did not affect those measurements. Before each experiment, the tank was stirred to ensure an even distribution of particles. Fluid movement in the tank was allowed to settle for at least 3 min, or until we could no longer visually identify any bulk motion of oil or particles before beginning each tow.

A video camera (MotionScope PCI 1000s camera; Redlake, Inc., Tucson, AZ) was used to record images (480 × 420 pixels) of the positions of the marker particles in the oil surrounding the model. The video camera was mounted on the rail system and towed along with a model to record particles moving in relation to the model. During tows, the camera also recorded particles illuminated in a horizontal plane of light that showed fluid motion with a cross-sectional view of the model (Fig. 2), or was affixed to the side of the tank to record particles illuminated in a vertical plane of light showing fluid flow with a longitudinal view of the model. Images were captured at a rate of 60 fps.

Video images were processed using MatPIV 1.6.1 software written for Matlab (Sveen, 2004), based on a method developed by Cowen and Monismith (1997). This software divided each video frame into an array of interrogation sub-windows (8 × 8 pixels), then used cross-correlation analysis to calculate the most probable displacement of particles in each sub-window in successive pairs of video frames. These displacements were used to calculate the local fluid velocity vectors for each sub-window in the fluid around the model. For each model tow, termed a "run," we performed PIV analysis of 60 image pairs when the model was in the middle third of the tank and the flow had reached steady state. For each run, we calculated the mean x and y components of the velocity (u and v, respectively) for each sub-window ($n = 60$ image pairs). We ran three replicate runs per treatment tested. The vector sum of the grand mean of u and the grand mean of v in each sub-window was used to determine the mean resultant fluid velocity in the sub-window. The velocity vectors computed using particle motions around the scaled-model were then converted using *Re* scaling to the velocities of water in relation to the dimensions of a real antennule. The shadings in Figures 3C and E reflect the magnitudes of those grand mean local velocity vectors (*i.e.*, mean local water speeds in relation to the antennule).

PIV analyses of the flow relative to cross-sectional views (Fig. 3) and to longitudinal views of the lateral flagellum were performed for each of the *Re*'s listed in Table 1 for both the splayed and the clumped models. We found no flow along the long axis of the flagellum except at the very distal tip of the model. Therefore, our measurements of fluid velocities in the cross-sectional plane at the middle of the model represent the flow through the majority of the aesthetasc array for all of the treatments tested in our experiments.

Since aesthetascs splay during the rapid flick downstroke and clump together during the slower return stroke, the area of the aesthetasc array in the plane of laser light differed between the downstroke and the return stroke. Thus, for each run, we transformed the actual coordinates of the aesthetascs in our video images (Fig. 3A–C) into a rectilinear grid ("*S* coordinates" for the x-axis, and "*T* coordinates" for the y-axis; Fig. 3D–F); this enabled easy comparison of the flow through comparable positions within the aesthetasc array for the downstroke and return stroke. The rectilinear grid, which encompassed only the area of the aesthetasc array (shown by the gray box in Fig. 3C, E), had 100 × 100 grid points. For each run, the u and v components of velocity at each of these grid points was interpolated from the PIV data (using the low-pass interpolation algorithm in Matlab), from which the resultant velocity vector at each grid point was calculated. Figures 3E and F represent the

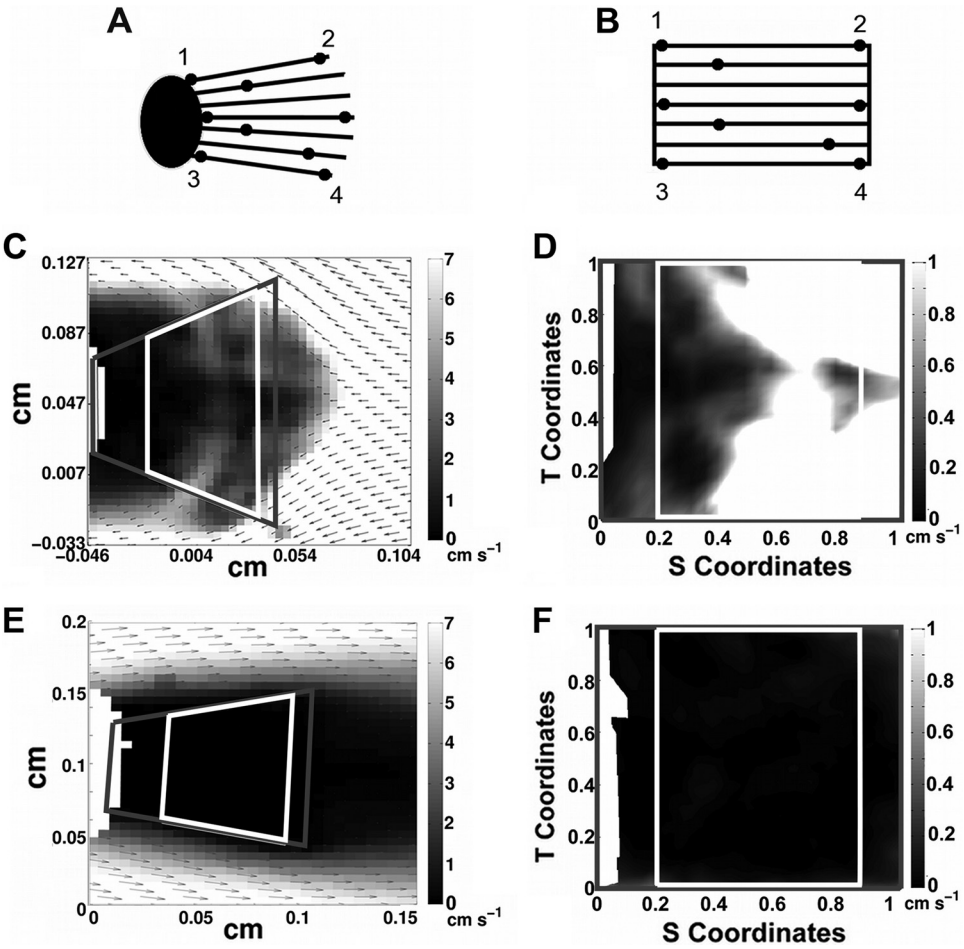

Figure 3. Cross-sectional views of water flow through the modeled aesthetasc array of the lateral flagellum of *Callinectes sapidus*. (A) Diagram of an antennule as recorded by the camera. The black oval represents the lateral flagellum, the lines are aesthetascs, and the black dots show arbitrary positions along the aesthetascs. (B) Because the area of the aesthetasc array (gray boxes in (C) and (E)) changes between the downstroke and return stroke, we transformed the actual coordinates of the aesthetascs into a rectilinear grid, as diagrammed. Points 1–4 represent the new, transformed positions of the arbitrary points 1–4 labeled in (A). The black dots and lines denote the same positions and aesthetascs as in (A). (C) Map of velocity vectors (black arrows) in relation to the antennule as measured by particle image velocimetry (PIV) for the splayed model moving at the *Re* of the downstroke in still water. The antennule is moving from left to right; thus, the flow moves from right to left. The size scales were converted to the dimensions of a real antennule, and the fluid speeds (represented by shadings) were converted to the speeds of water relative to a real antennule. The gray box indicates the bounds of the aesthetasc array; the white box denotes the dendrite-bearing region of the aesthetascs within the array. (D) Water speed during the downstroke within the aesthetasc array, interpolated onto the standardized grid from data shown in the gray box in (C). The white box indicates the dendrite-bearing area of the aesthetasc array. (E) Map of velocity vectors from PIV for the clumped model moving at the *Re* of the return stroke. The antennule is moving from right to left, so the flow in relation to it is moving from left to right. Boxes and scales are as in (C). (F) Water speed during the return stroke within the aesthetasc array, interpolated onto the standardized grid from data shown in the gray box in (E).

mean magnitudes of those vectors at each grid point ($n = 3$ replicate runs).

When calculating mean water speeds in the aesthetasc array, we used only those velocity vectors measured in the area of the array where the dendrites of the chemosensory neurons are located, because that is the region in which the odorant molecules captured at aesthetasc surfaces can diffuse to receptors. For *C. sapidus*, there are no dendrites in the proximal 28% or the distal 11% of an aesthetasc's length (Gleeson *et al.*, 1996). The white box in Figure 3C and E denotes the dendrite-containing area of the aesthetasc array, while the white box in Figures 3E and F shows the dendrite-containing area in the rectilinear grid of the array. For each run, we used the magnitudes of the velocity vectors at the 6100 grid

points within the white box to calculate the mean speed of the water in the dendrite-containing region of the aesthetasc array. For each treatment, we calculated the grand mean of those mean water speeds ($n = 3$ replicate runs).

Fraction of aesthetasc array refreshed with new water during a flick

For each run, we used the mean velocities (*e.g.*, Fig. 3C, E) to calculate an estimate of the fraction of the dendrite-containing area of the aesthetasc array (*e.g.,* area inside the white box in Fig. 3C, E) that was refreshed with a new water sample during a downstroke or a return stroke. A sub-window in the dendrite-containing area was considered "refreshed" if the parcel of water that occupied it at the start of the stroke had exited the dendrite-containing area of the aesthetasc array by the end of the stroke. We divided the period of a stroke into 50 time steps, assumed that the flow through the array was steady, and used a forward Euler approximation to find the positions of each fluid parcel at each time step (*e.g.,* Kundu and Cohen, 2008). Specifically, during the first time step, a parcel of water in each PIV sub-window was advanced to a new position by multiplying the velocity vector in that sub-window by the time step. The velocity vector at the new position of each parcel was then multiplied by the time step to move each parcel to its next position, and so on. The parcel's local vector was calculated using a low-pass interpolation algorithm if the position of a water parcel fell between the positions of two measured vectors. We determined which parcels of water were at positions outside the dendrite-containing area of the aesthetasc array at the end of the 50 time steps in the stroke (*i.e.*, those parcels that had exited that area). We divided the number of water parcels that had exited the array at the end of a stroke by the total number of parcels that were in the dendrite-containing area at the start of the stroke to determine the fraction of that area that had been refreshed.

Width of gaps between aesthetascs

We determined the mean width of the gaps between aesthetascs intersecting the cross-sectional plane at the middle of the clumped model, which was illuminated by the laser during the PIV measurements. The clumped model was partially immersed in oil so that the air-oil interface occurred at the plane that had been illuminated by the laser. The meniscus at the air-oil interface was visible around each Pyrex aesthetasc and photographed with a Canon Powershot A460 digital camera. The midpoint position of each aesthetasc was digitized, and the x and y coordinates of each aesthetasc midpoint were converted to the dimensions of a crab antennule to the nearest 0.01 μm using Image-J software (Abramoff *et al.*, 2004). We then calculated the distance between the midpoint of each aesthetasc and that of its nearest neighbor with the Matlab Delaunay triangulation method, which determines the position of the nearest point to each query point (in this case, the points were the midpoints of the aesthetascs). Gap width between each pair of aesthetascs was then calculated by subtracting the mean diameter of an aesthetasc (8.5 $\pm$ 2 mm, SD) from the distance between neighboring aesthetascs. The mean gap width was then calculated ($n = 197$ gap widths between nearest neighbors).

Statistical analyses

All statistical calculations (means, 95% confidence intervals, multi-way ANOVA) were done using *R* standard statistical package (R Development Core Team, 2011). We used a 3-way ANOVA with a Bonferroni correction to perform a pairwise comparison of water speeds within the array or fraction of the array refreshed, where the categories of variables tested were 1) configuration of the aesthetasc array (splayed *vs.* clumped), 2) orientation of the aesthetasc array on the lateral flagellum (upstream *vs.* downstream), and 3) Reynolds number (*Re* ranging from 0.23–2.8). We also used a 2-way ANOVA with a Bonferroni correction to test the fraction of the array refreshed against two categories: 1) the speed of the ambient current in which the antennule was flicked and 2) the stroke of the antennule. Comparisons were treated as significant if the *P*-value was less than 0.05.

Results

Sniffing by the antennules of blue crabs

Maps of the mean speeds of water flow in relation to the array of aesthetascs on the lateral flagellum of *Callinectes sapidus* during a flick downstroke and return stroke in still water are shown in Figure 3. During the downstroke, when the aesthetasc array was on the upstream side of the flagellum and the aesthetascs were splayed, water entered the upstream end of the array and exited *via* the sides of the array. The water flowing through the array moved more slowly than the water flowing around the antennule, and water speed in the array decreased with distance from the distal tips of the aesthetascs (Fig. 3C). Although water speeds were close to zero in the proximal region of the array, near the flagellum where the aesthetascs were very close to their neighbors, water flowed through the dendrite-bearing region of the aesthetasc array (Fig. 3D) at a mean speed of 1.43 cm s^{-1} (Table 1). In contrast, during the return stroke, when the aesthetascs were clumped together on the downstream side of the flagellum in its wake, most of the water flowed around rather than through the array of aesthetascs (Fig. 3). The slow flow through the array during the return stroke was in the opposite direction of the flow during the downstroke, and the mean velocity in the aesthetasc-bearing area of the array was only 0.04 cm s^{-1} (Fig. 3F; Table 1).

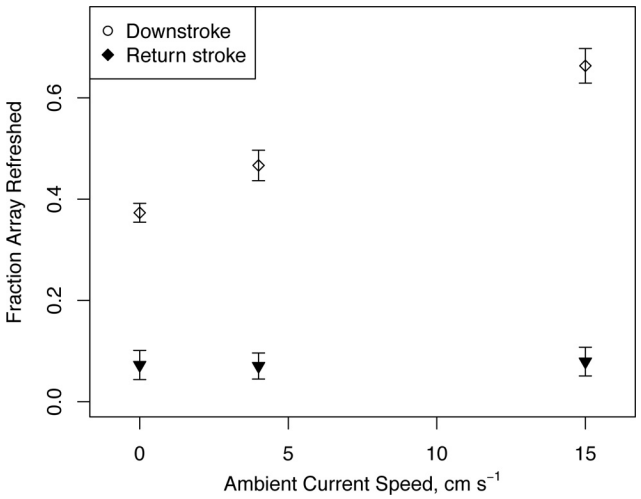

Figure 4. Grand mean (mean of three replicates) of the fraction of the dendrite-bearing area of the aesthetasc that was refreshed by new water during a downstroke (white diamonds) or recovery stroke (black triangles) of the lateral flagellum of a *Callinectes sapidus*, plotted as a function of the speed of the ambient water current encountered by the animal. The aesthetasc-bearing side of the lateral flagellum faced upstream into the ambient current. Error bars indicate standard deviations (SD).

The fraction of the dendrite-bearing area of the aesthetasc array that was refreshed by a new water sample during a flick downstroke or return stroke is plotted in Figure 4. During the downstroke in still water, 0.37 of the dendrite-bearing region was refreshed. In contrast, during the return stroke, only 0.07 of the dendrite-bearing area was refreshed. Thus, most of the new water that penetrated the aesthetasc array during the downstroke was retained within the array during the return stroke.

Callinectes sapidus often executes a series of antennule flicks at a frequency of 3 Hz, with a pause of approximately 0.24 s between the end of a return stroke and the start of the next downstroke (Reidenbach and Koehl, 2011). Therefore, a water sample trapped in the aesthetasc array at the end of the downstroke remains there during the 0.07-s duration of the return stroke plus the 0.24-s period of the pause. We calculated an estimate of the probability that odorant molecules in that trapped water sample can diffuse to the surfaces of aesthetascs before the next flick downstroke drives a new water sample into the aesthetasc array. The probability (P) that a diffusing molecule has traveled a distance between x and $[x + dx]$ from its starting point during a period of time (t) is given by

$$P(x)dx = \frac{1}{\sqrt{4\pi Dt}} e^{-x^2/4Dt} dx \qquad \text{(Equation 4)}$$

where D is the diffusion coefficient of the molecule (Berg, 1993). Amino acids, odorants to which crustaceans respond (*e.g.*, Hay, 2011), have diffusion coefficients in water of about 10^{-9} m^2 s^{-1} (Lide, 1991). During the return stroke and pause, the aesthetascs were in the clumped configuration (Fig. 1F, H), when the mean gap width between neighboring aesthetascs on our model corresponded to a mean gap width on a real antennule of 8.9 ± 4 μm (SD, n = 197 gap widths between nearest neighbors).

Therefore, the greatest distance that a molecule would have to diffuse to reach the surface of an aesthetasc would be 4.4 mm, the distance from the middle of the gap to the surface of an aesthetasc. Equation 4 was integrated to find the probability distribution of distances, x, to which molecules travel by molecular diffusion during the period when a water sample was trapped in the aesthetasc array (t = 0.31 s). For molecules starting at the midpoint of a gap (x = 0), the area under that probability distribution for all $x \leq -4.4$ mm and $x \geq 4.4$ mm gave a P-value of 0.929. This value indicated that an odorant molecule located at the middle of a gap between aesthetascs had a 92.9% chance of diffusing the distance to the surface of an aesthetasc during the return stroke and inter-flick pause. Odorant molecules in the water between aesthetascs that started at distances less than 4.4 mm from an aesthetasc had even higher probabilities of diffusing to an aesthetasc surface.

Our PIV data and diffusion estimates showed that 1) the lateral flagellum on the antennule of a *C. sapidus* forced a new water sample into the aesthetasc array during a flick downstroke and retained that sample during the return stroke and inter-flick pause; and 2) there was enough time during the return stroke and inter-flick pause for most of the odorant molecules in that water sample to diffuse to the surfaces of the aesthetascs before the next flick. Thus, our results indicated that the antennules of *C. sapidus* sniff when they flick.

Effects of splaying of aesthetascs on water flow through the array

To explore how water movement through the array of aesthetascs was affected by aesthetasc flexibility, we compared mean water speeds within the dendrite-containing area of the array of aesthetascs in the splayed configuration with the array in the clumped configuration when the aesthetascs moved at the same *Re* and orientation (Fig. 5, Table 1).

When the aesthetascs were on the upstream side of a lateral flagellum (*i.e.*, the orientation during a downstroke), water speeds within the array were significantly greater in the splayed array than in the clumped array for all *Re's* ≥ 1.6 ($F(1,10) = 11.7$, $P = 3.1 \times 10^{-5}$). In contrast, when the aesthetascs were on the upstream side of slowly moving antennules ($Re \leq 0.94$), splay did not affect water speeds within the aesthetasc array ($F(1,4) = 6.81$, $P = 0.53$). Similarly, when the aesthetascs were on the downstream side of a lateral flagellum (*i.e.,* the orientation during a return stroke), splay had no effect on water speeds in the array when the antennule moved slowly ($Re \leq 0.94$) ($F(1,4) = 64.76$, $P = 0.99$). Although water speeds in the

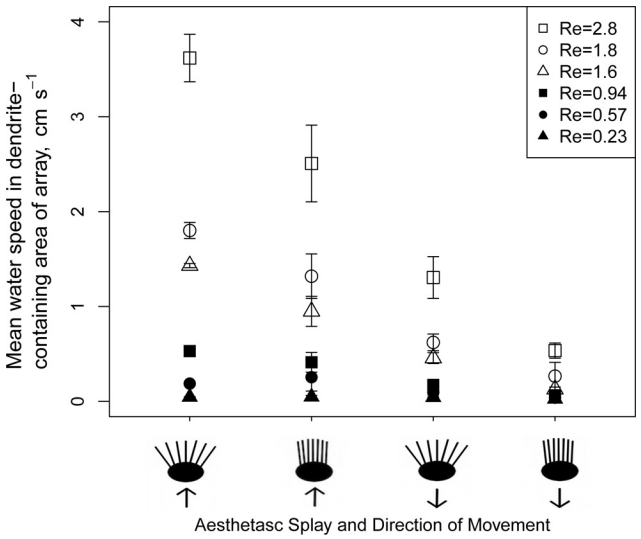

Figure 5. Grand mean water speed (mean of three replicates) within the dendrite-bearing area of the aesthetasc array of the lateral flagellum of the antennule of a *Callinectes sapidus*, plotted for different configurations of the aesthetasc array and directions of movement by the antennule. The black circles below the *x*-axis represent the lateral flagellum seen in cross-section; the lines emanating from each circle represent the aesthetascs in the splayed or the clumped configurations. Arrows indicate the direction in which the antennule is moving, with the aesthetasc array on the upstream side of the flagellum (the two diagrams on the left) or on the downstream side (the two diagrams on the right). The antennule strokes and ambient current conditions that produce these *Re*'s are listed in Table 1. Error bars represent standard deviations (SD).

splayed array on the downstream side of the antennule were significantly greater than when in the clumped array at $Re \geq 1.6$ ($F(1,4) = 422$, $P = 2.8 \times 10^{-8}$), the differences in speed were not as pronounced as when aesthetascs were on the upstream side of the flagellum. Thus, the increase in the width of the gaps between aesthetascs due to their flexibility only led to an increase in water speed within an array if the antennule moved rapidly (at *Re*'s similar to those of flick downstrokes).

If crab antennules were not flexible, they would remain in the clumped configuration on the upstream side of the antennule during the rapid downstroke ($Re = 1.6$). They would also be clumped when on the downstream side of the antennule during the slower return stroke ($Re = 0.57$). For these stiff aesthetascs, the mean speed in the dendrite-bearing area of the aesthetasc array for the downstroke was only 0.95 cm s^{-1}, which was significantly lower than the water speed (1.43 cm s^{-1}) in the splayed array of flexible aesthetascs during the downstroke (Fig. 5, Table 1).

Effects of upstream versus *downstream location of the aesthetasc array on water flow through the array*

To study how water flow through an array of aesthetascs was affected by antennule orientation, we compared mean water speeds within the dendrite-containing area of an array on the upstream *versus* the downstream side of the flagellum when it was moving at the same *Re* and held in the same configuration (*i.e.*, splayed or clumped) (Fig. 5, Table 1). When the antennule was in the splayed configuration, water speed in the aesthetasc array was significantly greater when it was on the upstream side than when on the downstream side of the antennule for $Re \geq 1.6$ ($F(1,10) = 261$, $P = 2.9 \times 10^{-7}$). However, orientation had no effect on water speed in the splayed aesthetasc array for $Re \leq 0.57$ ($F(1,4) = 12.4$, $P = 0.41$). Similarly, water flow was significantly faster in clumped arrays on the upstream side of the flagellum than on the downstream side when $Re \geq 0.94$, but not for $Re \leq 0.57$. Thus, positioning the aesthetasc array on the upstream, not the downstream, side of the lateral flagellum only led to an increase in water speed within an array if the antennule moved rapidly. Therefore, splaying did play a role in altering water speeds through the array during the downstroke when $Re = 1.6$, but it did not have a significant effect on water speed during the return stroke when $Re = 0.57$.

Effects of antennule speed on water flow through an array of aesthetascs

We explored how the difference in antennule speed alone between the downstrokes ($Re = 1.6, 1.8, 2.8$) and return strokes ($Re = 0.23, 0.57, 0.94$) of the lateral flagellum affected water flow through an array of aesthetascs. We compared mean water speeds within the dendrite-containing area of an array at the two *Re's* when the aesthetasc array was in the same configuration and orientation (Fig. 5, Table 1). With the antennule in the splayed configuration, the mean speed of water flow in the aesthetasc array was significantly greater at the *Re* of a downstroke than at the *Re* of a return stroke, when the aesthetasc array was on the upstream side of the antennule ($F(2,7) = 26.1$, $P = 0.024$), not when it was on the downstream side ($F(2,7) = 12.4$, $P = 0.16$). In contrast, when the aesthetasc array was in the clumped configuration and facing upstream, the speed of water in the array was not greater at the *Re* of the downstroke than at the *Re* of the return stroke ($F(2,7) = 4.17$, $P = 0.99$). Furthermore, when the clumped array was on the downstream side of the antennule, no difference was noted between the flow speed in the array when the antennule moved at the *Re* of the downstroke and at the *Re* of the return stroke ($F(2,7) = 8.27$, $P = 0.41$). Thus, the change in *Re* between the rapid downstroke and the slower return stroke was more effective at altering water speed within an aesthetasc array if the gaps between the aesthetascs were large (splay configuration) than if they were narrow (clumped configuration).

Effect of an ambient water current on flow through the array of aesthetascs

To test how ambient currents alter flow within the aesthetasc array, we altered the tow velocities of the antennule models to replicate the water velocities in relation to the antennules during the downstroke and the return stroke under ambient flow conditions of 4 cm s^{-1} and 15 cm s^{-1}. When it is exposed to ambient water flow, *Callinectes sapidus* orients the aesthetasc-bearing ventral surface of each antennule to face upstream, and flicks the lateral flagellum of each antennule at the downstroke and return stroke velocities listed in Table 1. Therefore, when a crab flicks the lateral flagellum of its antennule in an ambient water current, the net water velocity experienced by the flagellum is the vector sum of the ambient water velocity and of the water velocity in relation to the flagellum due to its flicking motion. In contrast, during the return stroke, the flagellum moves in the same direction as the ambient current, so that the water motion relative to the flagellum due to its motion is subtracted from the water flow past the flagellum due to the ambient current.

The mean water speeds within the dendrite-bearing area of the aesthetasc array during the downstroke (*i.e.,* splayed array facing upstream) were significantly greater in ambient currents of 4 cm s^{-1} (net $Re = 1.8$) and 15 cm s^{-1} (net $Re = 2.8$) than in still water ($Re = 1.6$) (Fig. 4) ($F(2,7) = 254$, $P = 1.6 \times 10^{-5}$). In contrast, mean water speeds in the clumped aesthetasc array during the return stroke were not affected by ambient currents. There were no significant differences between mean velocities within the array in still water at $Re = 0.57$ and in ambient currents of 4 cm s^{-1} (net $Re = 0.23$) or 15 cm s^{-1} (net $Re = 0.94$) (Fig. 4) ($F(2,7) = 10.4$, $P = 0.24$).

The fraction of the dendrite-bearing area of the aesthetasc array that was refreshed with a new water sample during a flick downstroke or recovery stroke is plotted as a function of ambient current speed in Figure 4. During the downstroke, the faster the ambient current, the greater the area of aesthetasc array that was refreshed, although these differences are marginally not significant ($F(2,7) = 19.7$, $P = 0.051$). In contrast, the fraction of the dendrite-bearing region of the array that was refreshed during the return stroke did not vary with ambient current velocity ($F(2,7) = 5.47$, $P = 0.88$). Therefore, the difference in area refreshed between the downstroke and the return stroke increased as ambient water speed was increased; ambient water flow enhanced the sniffing by antennules of *C. sapidus*.

Summary of factors affecting flow speeds within aesthetasc arrays

Overall, each of the variables tested significantly affected flow speed of the fluid within the dendrite-bearing section of the aesthetasc array (*Re*: $F(5,64) = 840$, $P < 1 \times 10^{-16}$; orientation to flow: $F(1,64) = 298$, $P < 1 \times 10^{-16}$; splaying of aesthetascs: $F(1,64) = 48.2$, $P = 2 \times 10^{-9}$). Interactions between *Re* and orientation ($F(5,64) = 252$, $P < 1 \times 10^{-16}$) and *Re* and splay ($F(5,64) = 50.7$, $P = 1 \times 10^{-9}$) were significant, while interactions between orientation and splay ($F(1,64) = 0.798$, $P = 0.38$) and all three variables did not reach significance ($F(5,64) = 2.39$, $P = 0.13$).

Discussion

Parameters that affect sniffing by aesthetasc-bearing olfactory antennules

Our study showed that when a blue crab *Callinectes sapidus* flicks the lateral flagellum of one of its olfactory antennules through the surrounding water, it captures a sample of that water in the spaces within the tuft of chemosensory sensilla (aesthetascs) that it bears. During the rapid downstroke of the flick, the closely spaced aesthetascs, which are on the upstream side of the lateral flagellum, splay passively because they are flexible. Water flows into the spaces between the aesthetascs in the array during the downstroke, then is retained within the array during the slower return stroke, when the aesthetascs are pushed together in a clump on the downstream side of the flagellum. There is enough time during the return stroke and inter-flick pause for most of the odorant molecules (≥92.9%) in that trapped water sample to diffuse to the surfaces of the aesthetascs before the next flick, when a new water sample is taken. Thus, an antennule of *C. sapidus* takes a discrete sample of ambient water and the odorants it carries each time it flicks.

The aesthetascs on the antennule of a blue crab operate at a range of Reynolds numbers (Table 1) in which the flow between neighboring aesthetascs is very sensitive to their spacing and to the speed of antennule motion (*e.g.,* Cheer and Koehl, 1987a). Using dynamically scaled physical models to study the hydrodynamics of crab antennules, we were able to measure separately the effects of different morphological and kinematic parameters on the flow of water around and through a brush-like array of aesthetascs. We found that the flexibility of aesthetascs has a large effect on water flow through a tightly spaced array of aesthetascs. Flexible aesthetascs splay during the downstroke, increasing the width of the gaps between them. Wider gaps can permit an increase in water speed within the dendrite-bearing area of the aesthetasc array, but only if the antennule moves rapidly (at $Re \geq 1.6$, like *Re*'s of flick downstrokes). Similarly, we discovered that positioning the aesthetasc array on the upstream rather than the downstream side of the lateral flagellum only causes an increase in water speed within an array if the antennule moves rapidly. Our measurements showed that the change in *Re* between the rapid downstroke and the slower return stroke ($Re = 0.57$)

of a flick is more effective at altering water speed within an aesthetasc array if the gaps between aesthetascs are large, not narrow.

Crabs in natural habitats are exposed to ambient water currents. When crabs flick their antennules in an ambient current, they align the aesthetasc-bearing side of each antennule upstream. Ambient currents increase both average fluid velocity within the aesthetasc array and the size of the area within the array that is refreshed with new water during the downstroke. Therefore, the difference in area refreshed between the downstroke and the return stroke increases as ambient water speed increases. In this way, ambient water flow enhances the effectiveness of discrete odor sampling by antennules of *C. sapidus*.

Antennule performance in environments where salinity varies

Callinectes sapidus lives in estuarine habitats containing water of varying salinity (*e.g.,* Gleeson *et al.,* 1997). Sudden exposure of an antennule to fresh water ablates the chemosensory dendrites within the cuticle shaft of an aesthetasc, causing a loss of function (Gleeson *et al.,* 1996). However, if the salinity around an antennule is reduced slowly, the outer dendritic segments of the chemosensory neurons retract into just the proximal ends of the aesthetascs near their attachment to the lateral flagellum (Gleeson *et al.,* 1996). In addition, cations (Na^+, Ca^{2+}, K^+) leak out of the aesthetascs and into the water within the aesthetasc array, thereby maintaining a favorable ionic and osmotic microenvironment around the aesthetascs (Gleeson *et al.,* 1997, 2000a, b). We found that the water flow between aesthetascs near their proximal ends was very slow, even during a flick downstroke (Fig. 3B, E), and that water in this region of the aesthetasc array was not refreshed during a flick. Therefore, when exposed to a low-salinity environment, dendrites retract into a region of the aesthetasc where a microenvironment of higher-salinity water can be maintained around the aesthetasc in the region of the array not refreshed during the downstroke.

Comparison of crab antennules to those of other malacostracan crustaceans

The short lateral flagellum of the antennule of a brachyuran crab, such as *Callinectes sapidus*, bears a densely packed tuft of aesthetascs (Fig. 1), while the long flagella of the antennules of stomatopods and lobsters bear rows of more widely spaced aesthetascs (reviewed by Koehl, 2006, 2011). Although these antennules are very different in morphology, they all have the ability to sniff (*i.e.,* take a discrete water sample with each flick and retain it in the aesthetasc array long enough for odorant molecules in the sample to diffuse to the aesthetascs) (reviewed by Koehl, 2006, 2011). Each species executes a flick downstroke at a *Re* high enough for water to flow between aesthetascs, depending on their spacing, and a return stroke at a *Re* low enough such that water flows around rather than through the spaces between aesthetascs. However, crab antennules have two features not shared by lobsters or stomatopods: 1) crab aesthetascs are flexible, while those of lobsters and stomatopods are stiff; and 2) the aesthetasc tuft of a crab is on the upstream side of the lateral flagellum during the downstroke and on the downstream side during the return stroke, whereas the rows of aesthetascs on the flagella of lobsters and stomatopods are oriented laterally during both strokes of a flick. Our study showed that both the flexibility and orientation of the aesthetascs of crab antennules enhance water flow into the very dense aesthetasc arrays during the downstroke, and retention of a water sample in the array during the return stroke.

Reidenbach and Koehl (2011) investigated how flicking antennules of different morphologies (the long antennules of spiny lobsters *Panulirus argus vs.* short antennules of blue crabs *Callinectes sapidus*) sampled the fluctuating odor signals at different positions in a turbulent odor plume. Short antennules of crabs intercepted odors during a lower percentage of their flicks and encountered lower peak concentrations than did the comparatively longer antennules of lobsters. However, because crabs flick at a higher frequency than lobsters (3 Hz *vs.* 2 Hz), the duration of odor-free gaps between encountered odor pulses (an important indicator of position in the odor plume) was similar for the two types of antennules.

Conclusions

Antennules of blue crabs, like those of other malacostracan crustaceans, take discrete samples of water during each flick by having a rapid downstroke, when water flows into the aesthetasc array, and a slow recovery stroke, when water is trapped in the array. However, in contrast to the antennules of lobsters and stomatopods, in the crab antennule flow differences through the more densely packed aesthetasc array between the downstroke and return stroke of a flick are enhanced by 1) flexibility of the aesthetascs, which splay during the downstroke and clump together during the return stroke; and 2) orientation of the antennule, such that the aesthetascs face upstream on the downstroke and downstream on the return stroke. Furthermore, under ambient currents (up to 15 cm s^{-1}), the flexibility of aesthetascs, in combination with the orientation of the aesthetasc array into the flow, enhance water flow through the aesthetasc array during the downstroke while still retaining water within the array during the return stroke.

Acknowledgments

We thank N. George for assistance with the tow tank experiments and D. Evangelista for advice on data analysis.

Funds for this study were provided by a National Science Foundation Grant [IOS-0842685] to M.A.R.K.; a James S. McDonnell Foundation Grant [21002091] to M.A.R.K.; the Virginia G. and Robert E. Gill Professorship to M.A.R.K.; an IGERT Traineeship to L.W. from a National Science Foundation IGERT Grant [DGE-0903711] to R. Full, M.A.R.K., R. Dudley, and R. Fearing; and a Postdoctoral Fellowship from the Miller Institute, University of California, Berkeley, to M.A.R.K.

Literature Cited

Abramoff, M. D., P. J. Magelhaes, and S. J. Ram. 2004. Image processing with ImageJ. *Biophotonics Int.* **11:** 36–42.

Ache, B. W. 1982. Chemoreception and thermoreception. Pp. 369–398 in *The Biology of Crustacea,* Vol. 3, *Neurobiology: Structure and Function*, H. L. Atwood and D. C. Sandeman, eds. Academic Press, New York.

Ache, B. W., and C. D. Derby. 1985. Functional organization of olfaction in crustaceans. *Trends Neurosci.* **8:** 356–360.

Atema, J. 1985. Chemoreception in the sea: adaptations of chemoreceptors and behavior to aquatic stimulus conditions. *Soc. Exp. Biol. Symp.* **39:** 387–423.

Atema, J. 1995. Chemical signals in the marine environment: dispersal, detection, and temporal signal analysis. *Proc. Natl. Acad. Sci. USA* **92:** 62–66.

Atema, J. 1998. Tracking turbulence: processing the bimodal signals that define an odor plume. *Biol. Bull.* **195:** 179–180.

Berg, H. 1993. *Random Walks in Biology,* 2nd ed. Princeton University Press, Princeton, NJ.

Cheer, A. Y. L., and M. A. R. Koehl. 1987a. Paddles and rakes: fluid flow through bristled appendages of small organisms. *J. Theor. Biol.* **129:** 17–39.

Cheer, A. Y. L., and M. A. R. Koehl. 1987b. Fluid flow through filtering appendages of insects. *IMA J. Math. Appl. Med. Biol.* **4:** 185–199.

Cowen, E. A., and S. G. Monismith. 1997. A hybrid digital particle tracking velocimetry technique. *Exp. Fluids* **22:** 199–211.

Devine, D. V., and J. Atema. 1982. Function of chemoreceptor organs in spatial orientation of the lobster, *Homarus americanus*: differences and overlap. *Biol. Bull.* **163:** 144–153.

Dickman, B. D., D. R. Webster, J. L. Page, and M. J. Weissburg. 2009. Three-dimensional odorant concentration measurements around actively tracking blue crabs. *Limnol. Oceanogr. Methods* **7:** 96–108.

Evangelista, D., G. Cardona, E. Guenther-Gleason, T. Huynh, A. Kwong, D. Marks, N. Ray, A. Tisbe, K. Tse, and M. A. R. Koehl. 2014. Aerodynamic characteristics of a feathered dinosaur measured using physical models. Effects of form on static stability and control effectiveness. *PLoS One* **9(1):** e85203. doi:10.1371/journal.pone.0085203.

Gleeson, R. A. 1980. Pheromone communication in the reproductive behavior of the blue crab, *Callinectes sapidus*. *Mar. Behav. Physiol.* **7:** 119–134.

Gleeson, R. A. 1982. Morphological and behavioral identification of the sensory structures mediating pheromone reception in the blue crab, *Callinectes sapidus*. *Biol. Bull.* **163:** 162–171.

Gleeson, R. A., W. E. S. Carr, and H. G. Trapido-Rosenthal. 1993. Morphological characteristics facilitating stimulus access and removal in the olfactory organ of the spiny lobster, *Panulirus argus*: insight from the design. *Chem. Senses* **18:** 67–75.

Gleeson, R. A., L. M. McDowell, and H. C. Aldrich. 1996. Structure of the aesthetasc (olfactory) sensilla of the blue crab, *Callinectes sapidus*: transformations as a function of salinity. *Cell Tissue Res.* **284:** 279–288.

Gleeson, R. A., M. G. Wheatly, and C. L. Reiber. 1997. Perireceptor mechanisms sustaining olfaction at low salinities: insight from the euryhaline blue crab *Callinectes sapidus. J. Exp. Biol.* **200:** 445–456.

Gleeson, R. A., K. Hammar, and P. J. S. Smith. 2000a. Sustaining olfaction at low salinities: mapping ion flux associated with the olfactory sensilla of the blue crab *Callinectes sapidus*. *J. Exp. Biol.* **203:** 3145–3152.

Gleeson R. A., L. M. McDowell, H. C. Aldrich, K. Hammar, and P. J. S. Smith. 2000b. Sustaining olfaction at low salinities: evidence for a paracellular route of ion movement from the hemolymph to the sensillar lymph in the olfactory sensilla of the blue crab *Callinectes sapidus. Cell Tissue Res.* **301:** 423–31.

Goldman, J. A., and M. A. R. Koehl. 2001. Fluid dynamic design of lobster olfactory organs: high speed kinematic analysis of antennule flicking by *Panulirus argus*. *Chem. Senses* **26:** 385–398.

Goldman, J. A., and S. N. Patek. 2002. Two sniffing strategies in palinurid lobsters. *J. Exp. Biol.* **205:** 3891–3902.

Grünert, U., and B. W. Ache. 1988. Ultrastructure of the aesthetasc (olfactory) sensilla of the spiny lobster *Panulirus argus*. *Cell Tissue Res.* **251:** 95–103.

Hay, M. E. 2011. Crustaceans as powerful models in aquatic chemical ecology. Pp. 41–162 in *Chemical Communication in Crustaceans,* T. Breithaupt and M. Thiel, eds. Springer Verlag, New York.

Keller, T. A., I. Powell, and M. J. Weissburg. 2003. Role of olfactory appendages in chemically mediated orientation of blue crabs. *Mar. Ecol. Prog. Ser.* **261:** 217–231.

Koehl, M. A. R. 1995. Fluid flow through hair-bearing appendages: feeding, smelling and swimming at low and intermediate Reynolds numbers. *Soc. Exp. Biol. Symp.* **49:** 157–182.

Koehl, M. A. R. 1996. Small-scale fluid dynamics of olfactory antennae. *Mar. Freshw. Behav. Physiol.* **27:** 127–141.

Koehl, M. A. R. 2001. Fluid dynamics of animal appendages that capture molecules: arthropod olfactory antennae. Pp. 97–116 in *Computational Modeling in Biological Fluid Dynamics*, L. J. Fauci and S. Gueron, eds. Springer, New York.

Koehl, M. A. R. 2003. Physical modeling in biomechanics. *Philos. Trans. R Soc. Ser. B Biol. Sci.* **358:** 1589–1596.

Koehl, M. A. R. 2006. The fluid mechanics of arthropod sniffing in turbulent odor plumes. *Chem. Senses* **31:** 93–105.

Koehl, M. A. R. 2011. Hydrodynamics of sniffing by crustaceans. Pp. 85–102 in *Chemical Communication in Crustaceans,* T. Breithaupt and M. Thiel, eds. Springer Verlag, New York.

Kundu, P. K., and I. M. Cohen. 2008. *Fluid Mechanics,* 4th ed. Elsevier, Waltham, MA.

Lide, D. R. 1991. *CRC Handbook of Chemistry and Physics*. 72nd ed. CRC Press, Boca Raton, FL.

Loudon, C., and A. Tordesillas. 1998. The use of the dimensionless Womersley number to characterize the unsteady nature of internal flow. *J. Theor. Biol.* **191:** 63–78.

Loudon, C., B. A. Best, and M. A. R. Koehl. 1994. When does motion relative to neighboring surfaces alter the flow through arrays of hairs? *J. Exp. Biol.* **193:** 233–254.

Mead, K. S. 2002. From odor molecules to plume tracing: an interdisciplinary, multilevel approach to olfaction in stomatopods. *Integr. Comp. Biol.* **42:** 258–264.

Mead, K. S., and M. A. R. Koehl. 2000. Stomatopod antennule design: the asymmetry, sampling efficiency, and ontogeny of olfactory flicking. *J. Exp. Biol.* **203:** 3795–3808.

Mead, K. S., M. A. R. Koehl, and M. J. O'Donnell. 1999. Stomatopod sniffing: the scaling of chemosensory sensillae and flicking behavior with body size. *J. Exp. Mar. Biol. Ecol.* **241:** 235–261.

Mead, K. S., M. B. Wiley, M. A. R. Koehl, and J. R. Koseff. 2003.

Fine-scale patterns of odor encounter by the antennules of mantis shrimp tracking turbulent plumes in wave-affected and unidirectional flow. *J. Exp. Biol.* **206:** 181–193.

Moore, P., and J. Crimaldi. 2004. Odor landscapes and animal behavior: tracking odor plumes in different physical worlds. *J. Mar. Syst.* **49:** 55–64.

Moore, P. A., and K. E. Kraus-Epley. 2013. The impact of odor and ambient flow speed on the kinematics of the crayfish antennular flick: implications for sampling turbulent odor plumes. *J. Crust. Biol.* **33:** 772–783.

Moore, P. A., J. Atema, and G. A. Gerhardt. 1991. Fluid dynamics and microscale chemical movement in the chemosensory appendages of the lobster, *Homarus americanus*. *Chem. Senses* **16:** 663–674.

Munk, J. D. 2011. The descent of ant. Ph.D. thesis, University of California, Berkeley.

Nelson, J. M., DeF. Mellon, Jr., and M. A. Reidenbach. 2013. Effects of antennule morphology and flicking kinematics on flow and odor sampling by the freshwater crayfish, *Procambarus clarkii*. *Chem. Senses* **38:** 729–741.

Page, J. L., B. D. Dickman, D. R. Webster, and M. J. Weissburg. 2011a. Getting ahead: context-dependent responses to odorant filaments drive along-stream progress during odor tracking in blue crabs. *J. Exp. Biol.* **214:** 1498–1512.

Page, J. L., M. J. Weissburg, D. B. Dickman, and D. R. Webster. 2011b. Staying the course: the role of chemical signal spatial properties in navigation through turbulent plumes. *J. Exp. Biol.* **214:** 1513–1522.

Pravin, S., and M. A. Reidenbach. 2013. Simultaneous sampling of flow and odorants by crustaceans can aid searches within a turbulent plume. *Sensors* **13:** 16591–16610.

Pravin, S., DeF. Mellon, Jr., and M. A. Reidenbach. 2012. Microscale fluid and odorant transport to antennules of the crayfish, *Procambarus clarkii*. *J. Comp. Physiol. A* **198:** 669–681.

R Development Core Team. 2011. R: A Language and Environment for Statistical Computing. R Foundation for Statistical Computing, Vienna, Austria [Online]. Available: http://www.r-project.org [2015, August 21].

Rathbun, M. 1896. The genus *Callinectes*. *Proc. U. S. Natl. Mus.* **18:** 349–375.

Reidenbach, M. A., and M. A. R. Koehl. 2011. The spatial and temporal patterns of odors sampled by lobsters and crabs in a turbulent plume. *J. Exp. Biol.* **214:** 3138–3153.

Reidenbach, M. A., N. George, and M. A. R. Koehl. 2008. Antennule morphology and flicking kinematics facilitate odour sampling by the spiny lobster, *Panulirus argus*. *J. Exp. Biol.* **211:** 2849–2858.

Schmitt, B. C., and B. W. Ache. 1979. Olfaction: responses of a decapod crustacean are enhanced by flicking. *Science* **205:** 204–206.

Schoenfeld, T. A. 2006. Introduction to special issue: what's in a sniff? *Chem. Senses* **31:** 91–92.

Schuech, R., M. Stacey, M. Barad, and M. A. R. Koehl. 2012. Numerical simulations of odorant detection by biologically inspired sensor arrays. *Bioinspir. Biomim.* **7:** 016001.

Snow, P. J. 1973. The antennular activities of the hermit crab*, Pagurus alaskensis* (Benedict). *J. Exp. Biol.* **58:** 745–765.

Stacey, M. T., K. S. Mead, and M. A. R. Koehl. 2002. Molecule capture by olfactory antennules: mantis shrimp. *J. Math. Biol.* **44:** 1–30.

Sveen, J. K. 2004. An introduction to MatPIV v. 1.6.1. Pp. 1–27 in *Mechanics and Applied Mathematics*, Vol. 2, Dept. of Mathematics, University of Oslo.

Vogel, S. 1994. *Life in Moving Fluids*. Princeton University Press, Princeton, NJ.

Waldrop, L. D. 2012. The fluid dynamics of odor capture by crabs. Ph.D. thesis, University of California, Berkeley.

Waldrop, L. D. 2013. Ontogenetic scaling of the olfactory antennae and flicking behavior of the shore crab, *Hemigrapsus oregonensis*. *Chem. Senses* **38:** 541–550.

Waldrop, L. D., R. M. Bantay, and Q. V. Nguyen. 2014. Scaling of olfactory antennae of the terrestrial hermit crabs *Coenobita rugosus* and *Coenobita perlatus* during ontogeny. *PeerJ* **2:** e535. doi: 10.7717/peerj.535.

Waldrop, L. D., M. Hann, A. K. Henry, A. Kim, A. Punjabi, and M. A. R. Koehl. 2015. Ontogenetic changes in the olfactory antennules of the shore crab, *Hemigrapsus oregonensis*, maintain sniffing function during growth. *J. R. Soc. Interface* **12:** doi: 10.1098/rsif.2014.1077.

Webster, D. R., and M. J. Weissburg. 2009. The hydrodynamics of chemical cues among aquatic organisms. *Annu. Rev. Fluid Mech.* **41:** 73–90.

Webster, D. R., S. Rahman, and L. P. Dasi. 2001. On the usefulness of bilateral comparison to tracking turbulent chemical odor plumes. *Limnol. Oceanogr.* **46:** 1048–1053.

Weissburg, M. J., and R. K. Zimmer-Faust. 1994. Odor plumes and how blue crabs use them to find prey. *J. Exp. Biol.* **197:** 349–375.

Weissburg, M., L. Atkins, K. Berkenkamp, and D. Mankin. 2012. Dine or dash? Turbulence inhibits blue crab navigation in attractive-aversive odor plumes by altering signal structure encoded by the olfactory pathway. *J. Exp. Biol*. **215:** 4175–4182.